Journal of Controlled Release 347 (2022) 68–77

Contents lists available at ScienceDirect

Journal of Controlled Release

journal homepage: www.elsevier.com/locate/jconrel

ApoE-mediated systemic nanodelivery of granzyme B and CpG for enhanced glioma immunotherapy

Jingjing Wei [a], Di Wu [b], Yu Shao [c], Beibei Guo [a,d], Jingjing Jiang [a,d], Jian Chen [b,e], Jinping Zhang [c], Fenghua Meng [a,d,*], Zhiyuan Zhong [a,d,*]

[a] Biomedical Polymers Laboratory, College of Chemistry, Chemical Engineering and Materials Science, State Key Laboratory of Radiation Medicine and Protection, Soochow University, Suzhou 215123, PR China
[b] Institute of Functional Nano & Soft Materials (FUNSOM), Soochow University, Suzhou, 215123, PR China
[c] Institutes of Biology and Medical Sciences (IBMS), Soochow University, Suzhou 215123, PR China
[d] College of Pharmaceutical Sciences, Soochow University, Suzhou 215123, PR China
[e] Chinese Institute for Brain Research, Beijing, Research Unit of Medical Neurobiology, Chinese Academy of Medical Sciences, 102206, PR China

ARTICLE INFO

Keywords:
Glioma
Protein delivery
Blood-brain barrier
CpG ODN
Immunotherapy

ABSTRACT

The response of malignant glioma to immunotherapy remains gloomy due to its discrete immunological environment and poor brain penetration of immunotherapeutic agents. Here, we disclose that ApoE peptide-mediated systemic nanodelivery of granzyme B (GrB) and CpG ODN co-stimulates enhanced immunotherapy of murine malignant LCPN glioma model. ApoE peptide-functionalized polymersomes encapsulating GrB (ApoE-PS-GrB) could effectively penetrate the blood-brain barrier-mimicking endothelial cell monolayer *in vitro* and further be taken up by LCPN cells, inducing strong immunogenic cell death (ICD). The co-administration of ApoE-PS-GrB and ApoE-PS-CpG in orthotopic LCPN glioma-bearing mice co-stimulated cytokine production, maturation of dendritic cells (DCs), infiltration of cytotoxic T lymphocytes (CTLs) while reduction of regulatory T lymphocytes (T_{reg}) and M2 phenotype macrophages in the tumor microenvironment, leading to greatly delayed tumor progression and significantly prolonged survival time compared with all controls. The ApoE-mediated systemic nanodelivery of GrB and CpG ODN opens a new pathway for potent immunotherapy of malignant glioma.

1. Introduction

Glioma is the most common and malignant brain cancer that causes particularly poor patient survival [1,2]. The aggressive infiltration of glioma cells into the central nervous system refrains current medical practice including surgery and radiotherapy from complete tumor ablation. The efficacy of chemotherapy of glioma is, on the other hand, restricted by the blood-brain barrier (BBB) and systemic toxicities [3–5]. The immunotherapy that activates host's immune system to repress or eliminate tumor is considered as a promising treatment strategy for solid tumors including glioma [6–8]. Different groups reported that localized immunotherapy after surgery and/or in combination with radiotherapy could significantly improve the survival of glioma mice model [9–11]. The response of malignant glioma to systemic and subcutaneous immunotherapy remains, however, gloomy due to its discrete immunological environment and poor brain penetration of immunotherapeutic agents [12–14].

The immunotherapy of glioma can be augmented via inducing immunogenic cell death (ICD) with several chemotherapeutic agents such as doxorubicin [15], oxaliplatin [16] and cyclophosphamide [17]. The low glioma-selectivity coupled with severe toxic effects, nevertheless, greatly compromises the therapeutic outcomes [18,19]. It is difficult for cytotoxic drugs to achieve strong ICD of glioma without causing detrimental effects to the major organs and immune systems. In comparison, apoptotic protein drugs with a high specificity and activity have generally less off-target toxicity and better safety [20,21]. It is surprising to note that there are little studies on apoptotic proteins for immunotherapy of glioma. Granzyme B (GrB) is a key mediator of natural killer (NK) cells and cytotoxic T lymphocytes (CTLs) [22,23]. GrB is shown to kill tumor cells through attacking mitochondria and releasing cytochrome C and adenosine triphosphate (ATP) [24], which might generate specific tumor antigens. The immunotherapy of glioma might further be

* Corresponding authors at Biomedical Polymers Laboratory, College of Chemistry, Chemical Engineering and Materials Science, State Key Laboratory of Radiation Medicine and Protection, Soochow University, Suzhou 215123, PR China.
E-mail addresses: fhmeng@suda.edu.cn (F. Meng), zyzhong@suda.edu.cn (Z. Zhong).

https://doi.org/10.1016/j.jconrel.2022.04.048
Received 14 December 2021; Received in revised form 14 April 2022; Accepted 28 April 2022
Available online 6 May 2022

augmented via activating dendritic cells (DCs) with immunoadjuvants like CpG oligonucleotide (CpG) and R837 [25,26]. The immunoadjuvants were typically administered via intracranial (i.c.) injection or convection enhanced delivery (CED) [27], which not only requires special operative technique but also is often accompanied with brain edema and inflammation [28].

In this article, we report that apolipoprotein E peptide (sequence: LRKLRKRLLLRKLRKRLLC, ApoE)-mediated glioma delivery of GrB and CpG adjuvant co-stimulates a potent systemic immunotherapy of orthotopic malignant LCPN mouse model (Scheme 1). Apolipoprotein E known to mediate lipid delivery into brain via the low-density lipoprotein receptor (LDLR) and the LDLR related protein (LRP-1 and LRP-2) receptors is a natural protein that can efficiently cross BBB via transcytosis. Interestingly, many glioma cells were also found over-expressing LDLR, LRP-1 and/or LRP-2. The functionalization of nanosystems with recombinant apolipoprotein E via either adsorption, direct coating or covalent bonding appears an interesting strategy to enhance BBB penetration and anti-glioma therapy [29]. The large apolipoprotein E (ca. 34 kDa), however, poses significant challenges on production, conjugation, purification and stability in addition to potential immunogenic concerns. The short ApoE peptide (ca. 1.8 kDa) is less immunogenic, easy to synthesize, and amenable to different chemical

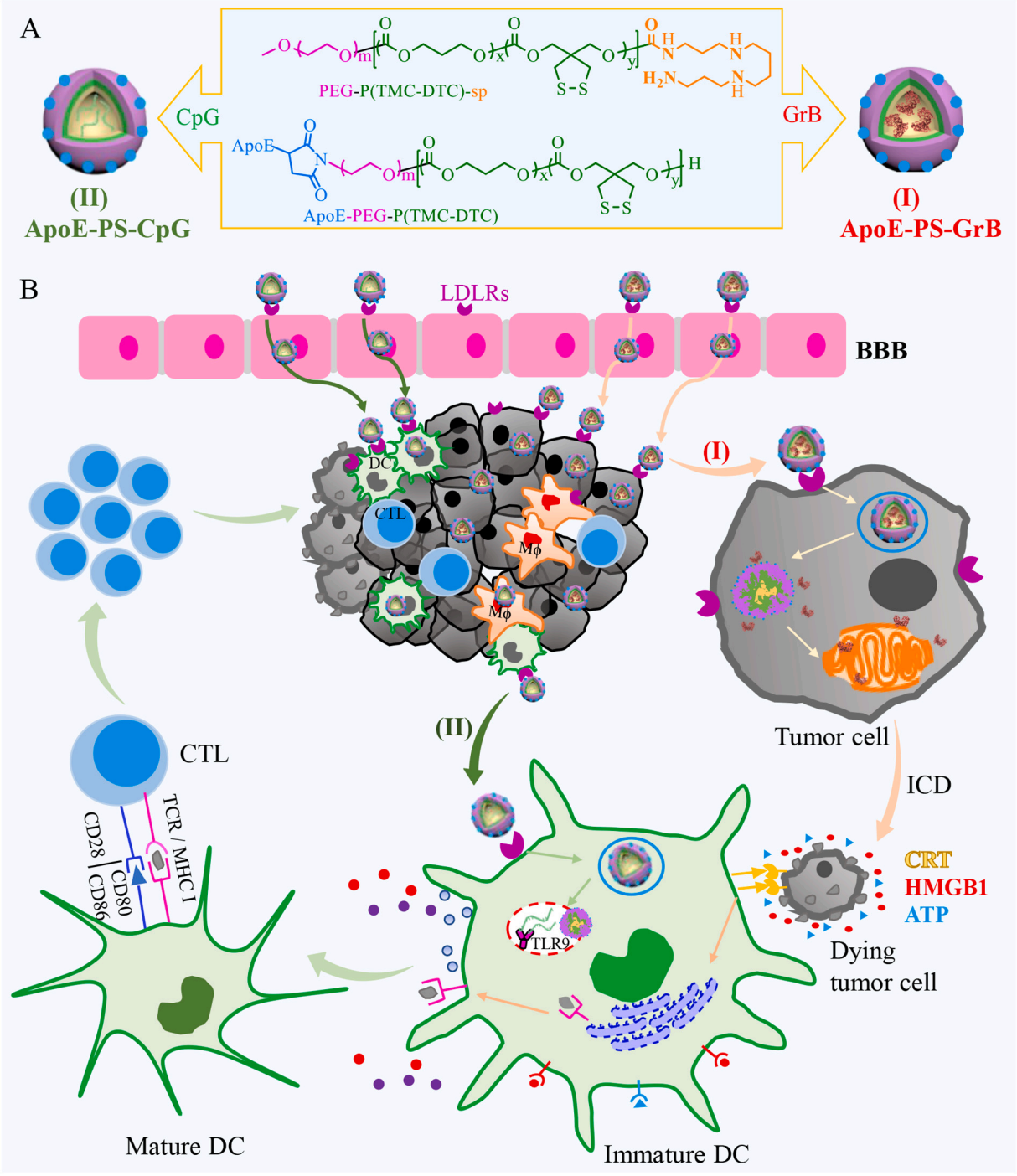

Scheme 1. Illustration of fabrication of ApoE peptide-functionalized polymersomes encapsulating GrB or CpG ODN (ApoE-PS-GrB and ApoE-PS-CpG) (A) and highly enhanced immunotherapy of murine orthotopic LCPN glioma (B).

manipulation. We have shown previously that the decoration of nanodrugs with ApoE peptide significantly elevates their BBB permeability and glioma targetability [30,31]. GrB encapsulated in ApoE peptide-functionalized polymersomes (ApoE-PS-GrB) effectively disrupts mitochondrion membrane of LCPN glioma cells and induces strong ICD and tumor associated antigens, which combining with systemic administration of ApoE-PS-CpG brings about greatly enhanced immunotherapy of murine glioma. The co-delivery of GrB and immunoadjuvants appears to be a promising immunotherapeutic modality for glioma.

2. Experimental section

2.1. Preparation of polymersomes loaded with GrB, CC or CpG

Typically, 50 μL DMSO solution of a mixture of ApoE-PEG-P(TMC-DTC) and PEG-P(TMC-DTC)-sp (both at 20 mg/mL) at 30/70, 20/80, 10/90 or 0/100 (mol/mol) was slowly injected into 950 μL HEPES buffer (5 mM, pH 6.8) that contained either GrB (10, 20 or 50 μg), CC (50, 100 or 150 μg), or CpG (100, 150 or 200 μg) under stirring (200 rpm, 10 min). The obtained dispersion was dialyzed (MWCO 350 kDa) sequentially against HEPES for 2 h, HEPES/PB (1/1, *v*/v) for 1 h, and PB for 2 h with medium exchange every hour. The drug loading efficiencies and contents of CpG were determined by using nanodrop and calculated from the standard curves of known concentrations, and those of GrB and CC were quantified by using fluorometry using Cy5 labeled GrB and CC (GrB-Cy5, CC-Cy5).

To study *in vitro* release of GrB, 500 μL ApoE-PS-GrB or PS-GrB (polymer concentration: 0.1 mg/mL) using GrB-Cy5 as model was transferred into dialysis tube (MWCO 350 kDa), and immersed in 20 mL PB (10 mM, pH 7.4) or PB containing 10 mM GSH in a shaking bath (200 rpm, 37°C). At desired time points, 5 mL dialysis medium was taken to quantify GrB-Cy5 released using fluorometry and 5 mL fresh medium was then added ($n = 3$).

2.2. Investigation on the in vitro BBB transcytosis of ApoE-PS-GrB

The simulated BBB model was built using bEnd.3 cell monolayer in a transwell as reported [32]. Briefly, into the donor chambers of the transwells were added Cy5-labed GrB, PS-GrB and ApoE-PS-GrB with ApoE content of 10%, 20%, and 30% (Cy5 concentration: 2 nM) at 37°C. The medium in bottom chamber was collected at 6, 12 and 24 h to quantify GrB-Cy5 using fluorometry, and an equal volume of fresh medium was replenished. The transport ratio was defined as the ratio of the drugs in the bottom to the total drugs added ($n = 3$).

2.3. Cellular uptake by LCPN cells

To quantify the expression of LDLR and LRP-2 on LCPN and bEnd.3 cells, total proteins were extracted and quantified by BCA protein assay kit, and equal amount of proteins were measured using western blot taking GAPDH as reference.

To study the receptor-mediated endocytosis, LCPN cells in serum-free DMEM/F12 containing N2 and B27 with EGF and bFGF as growth factors were seeded in a Matrigel-pretreated 6-well plate (1.5×10^5 cells/well) and cultured overnight. Cy5-labeled GrB, PS-GrB, ApoE-PS-GrB with ApoE of 10%, 20% or 30% (Cy5: 2 nM) was then added and incubated for 4 h at 37°C. LCPN cells were digested by accutase and collected for flow cytometric analysis and analyzed using FlowJo v10. The inhibition experiment was carried out by pretreating LCPN cells with free ApoE (final concentration: 20 μg/mL) for 2 h prior to the incubation with Cy5-labeled ApoE-PS-GrB (Cy5 conc.: 2 nM).

2.4. Cytotoxicity assays of ApoE-PS-GrB

LCPN cells were seeded in a Matrigel-pretreated 96-well plate (1×10^3 cells/well) overnight. 10 μL free GrB, PS-GrB or ApoE-PS-GrB (GrB conc.: 0.39–100 nM) was incubated for 72 h. Then 10 μL CCK-8 (5 mg/mL) was added to incubate for 2 h before measurement using a microplate reader. The cell viability (%) was determined by comparing the absorbance at 450 nm with control wells cultured with PBS (100% viability).

2.5. Endosomal escape evaluation and mitochondrial membrane destabilization

LCPN cells were cultured on glass coverslips in 24 well plates (5×10^4 cells/well) for 24 h. Cy5-labeled cytochrome C (CC-Cy5) was used as model. Cy5-labeled free CC, PS-CC, and ApoE-PS-CC (CC conc.: 4 μM) were added to culture for 4, 8 or 12 h. After incubation, the cells were fixed using 4% paraformaldehyde, and the endo/lysosomes and nuclei were stained with Lyso-tracker green and 4′,6-diamidino-2-phenylindole (DAPI), respectively. The fluorescence images were taken by CLSM. The Pearsons' colocalization coefficients of proteins and endo/lysosomes in the merged images were evaluated using Image J.

To study the effect on mitochondria, LCPN cells on coverslips in 24-well plate were incubated with free GrB, PS-GrB, or ApoE-PS-GrB (GrB conc.: 30 nM) for 24 h. The cells were then stained with MitoCapture and DAPI according to the manuals before CLSM observation. The fluorescence intensity ratio of destabilized to intact mitochondrial membrane (Green/Red) was semi-quantified by Image J.

2.6. The production of CRT, HMGB1 and ATP of LCPN cells in vitro

LCPN cells (2×10^5 cells/well) cultured in 6-well plates were incubated with GrB, PS-GrB, or ApoE-PS-GrB (GrB conc.: 30 nM) in 1 mL DMEM/F12 medium for 48 h ($n = 3$). Then, the culture medium was taken to quantify HMGB1 and ATP by ELISA kits and enhanced ATP assay kit, respectively. And the cells were digested by accutase, and incubated sequentially with anti-CRT monoclonal primary antibody and Alexa fluor 633-conjugated monoclonal secondary antibody for 20 min at 4°C before flow cytometry.

2.7. BMDC and BMDM activation in vitro stimulated by CpG formulations

Bone marrow-derived dendritic cells (BMDCs) and macrophages (BMDM) (5×10^5 cells/well) were all separately cultured in 6-well plates overnight before 24-h incubation with free CpG, PS-CpG or ApoE-PS-CpG (CpG conc.: 0.4 μg/mL) in 1 mL RPMI 1640 medium at 37°C ($n = 3$). The corresponding empty PS and ApoE-PS as well as PBS were used as control. Then BMDCs were stained with anti-CD11c-FITC, anti-CD80-APC, and anti-CD86-PE antibodies, and BMDM were stained with anti-CD11b-FITC, anti-F4/80-PE, and anti-CD206-Alexa fluor 647 antibodies for flow cytometry measurement.

2.8. In vivo pharmacokinetics of protein loaded polymersomes in mice

All animal procedures were handled under protocols approved by Soochow University Laboratory Animal Center, and the Animal Care and Use Committee of Soochow University. Healthy C57BL/6 mice were administered with 200 μL Cy5-labeled free CC, PS-CC, or ApoE-PS-CC (0.5 μmol CC-Cy5 equiv./kg) in PBS via tail veins ($n = 3$). At preset timepoints, ca. 60 μL blood was taken from retro-orbital sinus into heparinized tube. After centrifugation (3000 rpm, 10 min), 20 μL plasma was taken to incubate for 24 h with 700 μL DMSO solution (containing 20 mM DTT) in a shaking bath (37°C, 200 rpm) to extract CC-Cy5. The concentration of extract CC-Cy5 was measured using fluorometry and calculated based on the calibration curve of CC-Cy5 of known concentrations which underwent the same treatments as blood samples. The CC-Cy5 concentration in plasma was plotted against time, and using Software PK Solver the elimination half-lives and area under the curve (AUC) were analyzed.

2.9. In vivo therapeutic efficacy of ApoE-PS-GrB and ApoE-PS-CpG

Orthotopic malignant LCPN glioma model was established in C57BL/6 mice by stereotactically injecting 5×10^4 LCPN cells in 5 μL PBS containing Matrigel (25 vol%) into the right striatum using a 26-gauge Hamilton syringe that remained in place for 5 min after injection. The coordinates were: 0.5 mm anterior, 1.9 mm lateral, and 3.1 mm deep. The day was designated as day 0. On day 5, 8, 11 and 14, 200 μL PBS, ApoE-PS-GrB (0.1 mg/kg), ApoE-PS-CpG (0.5 mg/kg), or combo group of ApoE-PS-GrB + ApoE-PS-CpG (0.1 mg/kg + 0.5 mg/kg) were intravenously administered ($n = 9$). The body weight was measured every 2 days, and normalized to the initial weights. On day 16, ca. 120 μL blood was taken from four mice to get plasma for quantifying TNF-α, IFN-γ and IL-6 using ELISA kits. The four mice were later (day 20) sacrificed for immunohistochemical analysis and for flow cytometric analysis of immune cells. The other five mice in the group were monitored for Kaplan-Meier survival curves and the mice was considered dead when the mice died or the body weight lost >30% or unresponsive.

On day 20 post-implantation, when the mice of PBS group displayed signs of neurological deficits, one mouse from each group were randomly selected and sacrificed, and the main organs and tumor-bearing brain were removed for histological analysis using hematoxylin and eosin (H&E) staining. The tumor slices were treated with terminal deoxynucleotidyl transferase-mediated nick end labeling (TUNEL) or with anti-CRT primary antibody and Alexa fluor 633 secondary antibody to characterize CRT expression.

On day 20 post-implantation, three mice from each group were euthanized, and tumors were excised and homogenized in cold PBS to obtain single-cell suspension. Next lysed red cells within them with Ammonium-Chloride-Potassium (ACK) lysis buffer, then stained with the corresponding antibodies according to the protocols before flow cytometric measurements and analysis using FlowJo v10 software. T cells: anti-CD3-FITC, anti-CD8-PE/Cy7 or anti-CD4-APC antibodies. T_{reg}: anti-CD3-FITC, anti-CD4-APC and anti-CD25-PE antibodies. Activated antigen presenting cells: anti-CD11c-PerCP-Cy5.5, anti-CD80-APC and anti-CD86-PE antibodies. Macrophages: anti-CD11b-FITC, anti-F4/80-APC, and anti-CD206-PE antibodies.

2.10. Statistical analysis

All data were represented as average value ± SD. The differences among groups were calculated by One-way ANOVA using Tukey's post-test and the difference in survival was evaluated by One-way ANOVA using log-rank (Mantel-Cox) by using GraphPad Prism 8. $^*p < 0.05$ means significant, $^{**}p < 0.01$, $^{***}p < 0.001$ and $^{****}p < 0.0001$ mean highly significant.

3. Results and discussion

3.1. Preparation of ApoE-PS-GrB

Granzyme B (GrB) plays a vital role in our immune system. GrB once introducing into cancer cells will quickly induce cell apoptosis via attacking mitochondrion and dumping of cytochrome C and adenosine triphosphate (ATP) [33]. The cell death caused by GrB is likely immunogenic. We have previously shown that hyaluronic acid and cell penetrating peptide-mediated delivery of GrB potently inhibited human multiple myeloma and lung tumor xenografts in nude mice, respectively [34,35]. The aim of this study was to investigate the immunotherapeutic effects of GrB (which has not been studied before) toward malignant glioma, for which BBB-permeable and glioma-targeted GrB nanoformulation, ApoE-PS-GrB, was prepared from co-self-assembly of PEG-P(TMC-DTC)-spermine (PEG: 5.0 kDa, P(TMC-DTC): 16.9 kDa), ApoE-modified PEG-P(TMC-DTC) (PEG: 7.5 kDa, P(TMC-DTC): 17.1 kDa) and GrB [31,34]. Of note, ApoE-PS-GrB exhibited high GrB loading efficiencies of 81–100% at theoretical loading contents (TLC) of 1–5 *wt*% (Table S1), as a result of electrostatic interaction and hydrogen bonding between protein and spermine in the inner shell [36,37] as well as the disulfide-crosslinking during the polymersome preparation. ApoE-PS-GrB showed small sizes (42–45 nm) and neutral surface charge (zeta potential of 1.06–2.02 mV) (Fig. 1A and Table S1). The *in vitro* release studies using Cy5-labeled GrB (GrB-Cy5) showed over 80% release of GrB-Cy5 from ApoE-PS-GrB under 10 mM GSH in 24 h (Fig. 1B). In contrast, less than 25% GrB-Cy5 was released under non-reductive condition, confirming reduction-triggered protein release behavior of ApoE-PS-GrB. The non-targeting control, PS-GrB, obtained from PEG-P(TMC-DTC)-spermine and GrB had very similar biophysical and protein release properties as ApoE-PS-GrB (Fig. 1A and Table S1).

3.2. BBB penetration, glioma-targetability and intracellular protein release

To deliver GrB to the cytosol of glioma cells, passing through BBB and entering glioma cells are challenging requirements [35,38]. We firstly investigated the BBB transport behavior of ApoE-PS-GrB using GrB-Cy5 as model protein and bEnd.3 murine endothelial cell monolayer as an *in vitro* BBB model. The results revealed that ApoE at surface densities of 20% and 30% markedly enhanced GrB penetration through bEnd.3 cell layer at all time points (Figs. 1C and S1), corroborating high transcytosis of ApoE-PS-GrB [31,39]. For instance, at 24 h, ApoE-PS-GrB with 20% and 30% ApoE had a transport ratio of ca. 25%, which was 2.5 and 5-fold that of non-targeted PS-GrB and free GrB, respectively.

We then studied the cellular uptake of ApoE-PS-GrB in murine malignant LCPN glioma cells. The expression of LDLR and LRP-2 in bEnd.3 cells and LCPN cells was analyzed by Western blot measurements. We and others have shown previously that bEnd.3 cells have a high expression of LDLRs [29,31,40]. Here, bEnd.3 cells were employed as a positive control. Interestingly, Fig. 1D displays that LCPN cells expressed considerably more LDLR and LRP-2 than bEnd.3 cells, supporting that LDLRs are suitable targets for LCPN glioma. Flow cytometric analyses showed that ApoE-PS-GrB with ApoE density of 10%, 20% and 30% had 2.9, 4.2, and 3.8-fold better uptake than PS-GrB, respectively, in LCPN cells (Fig. 1E). The internalization of ApoE-PS-GrB was drastically reduced when LCPN cells were pretreated with free ApoE peptide, verifying receptor-mediated uptake of ApoE-PS-GrB in LCPN cells. Hereafter, ApoE-PS with 20% ApoE density, which shows efficient BBB transcytosis and uptake by LCPN cells, was selected for further investigations. Intriguingly, Fig. 1F shows that ApoE-PS-GrB caused pronounced death of LCPN cells with an IC_{50} of 69.7 nM at 72 h incubation while PS-GrB and free GrB induced little toxicity even at 100 nM, confirming that ApoE-PS-GrB possesses good glioma-targetability and free GrB is non-toxic due to its incapability of entering cells. These results highlight the important role of active targeting in application of intracellular protein drugs [41].

To preclude the toxic influence of GrB at higher concentrations, we employed Cy5-labeled cytochrome C (CC-Cy5) that has good availability and similar isoelectric point to GrB but lower toxicity as a model protein for cellular uptake and *in vivo* pharmacokinetic studies. Fig. 2A reveals intense and widespread cytoplasmic Cy5 fluorescence in LCPN cells treated for 8 h with ApoE-PS-CC. In great contrast, little Cy5 fluorescence was discerned in LCPN cells treated with PS-CC and free CC. The co-localization parameter, Pearson's correlation coefficient between two variables for ApoE-PS-CC, analyzed from the merged images of proteins (Cy5) and endo/lysosomes (Lysotracker green) using Image J, decreased from 0.10, −0.03 to −0.34 with increasing incubation time from 4, 8 to 12 h (Fig. 2B), certifying efficient escape of proteins from endo/lysosomes.

3.3. Mitochondrial membrane destabilization and immunogenic cell death by ApoE-PS-GrB

To investigate the influence of ApoE-PS-GrB on mitochondria, LCPN

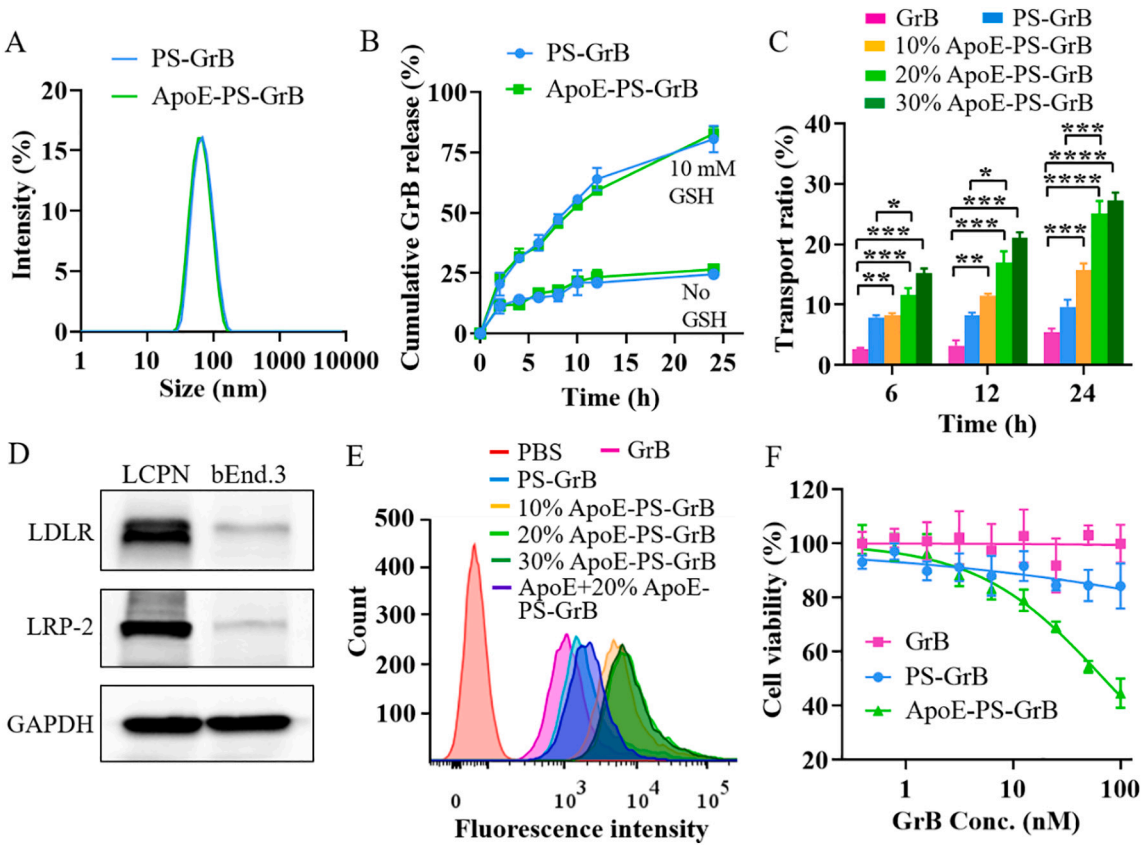

Fig. 1. (A) Size distribution profiles of PS-GrB and ApoE-PS-GrB. (B) *In vitro* release profiles of GrB-Cy5 from polymersomes in PB (10 mM, pH 7.4) with or without 10 mM GSH. (C) The transport ratio of GrB formulations from bEnd.3 cell monolayer at 6, 12 and 24 h incubation. (D) Western blot measurements of LDLRs expression on bEnd.3 and LCPN cells. (E) Flow cytometric analyses of the influence of ApoE surface densities on endocytosis by LCPN cells at 4 h incubation. (F) Cytotoxicity of LCPN cells co-cultured with ApoE-PS-GrB, PS-GrB or GrB for 72 h ($n = 3$). $^{*}p < 0.05$, $^{**}p < 0.01$, $^{***}p < 0.001$, $^{****}p < 0.0001$.

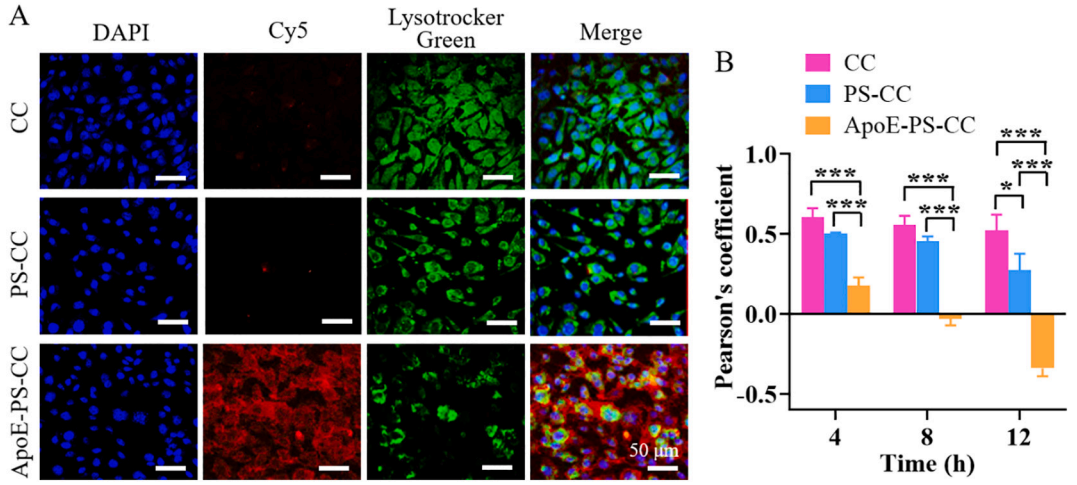

Fig. 2. The endosomal escape of CC-Cy5 loaded polymersomes ApoE-PS-CC and PS-CC in LCPN cells (CC-Cy5 conc.: 4 μM) observed by CLSM at 8 h incubation. (B) Pearson's correlation coefficient of CC-Cy5 and endo/lysosomes at 4, 8 or 12 h incubation analyzed using Image J. A Pearson's correlation coefficient of +1, 0 and −1 indicates strong positive correlation, no correlation and strong negative correlation, respectively. $^{*}p < 0.05$, $^{***}p < 0.001$.

cells following 24 h incubation with ApoE-PS-GrB were stained with MitoCapture. CLSM images displayed strong green fluorescence (i.e. monomer form in the cytosol) with little red fluorescence (i.e. aggregate form in the mitochondrial membrane) (Fig. 3A), indicating highly permeable mitochondrial membranes. In contrast, free GrB treated cells had intact mitochondrial membranes. PS-GrB caused some damages to mitochondrial membranes though obviously less than ApoE-PS-GrB. The semi-quantitative analyses confirmed that ApoE-PS-GrB brought about significantly increased Green/Red fluorescence intensity ratio compared to PS-GrB and free GrB (Fig. 3B). The destabilization of mitochondrial membrane by ApoE-PS-GrB would in turn lead to release of CC, ATP or effector substances [24], which can activate cascades of tumor cell death.

The destabilization of mitochondria membrane was reported to

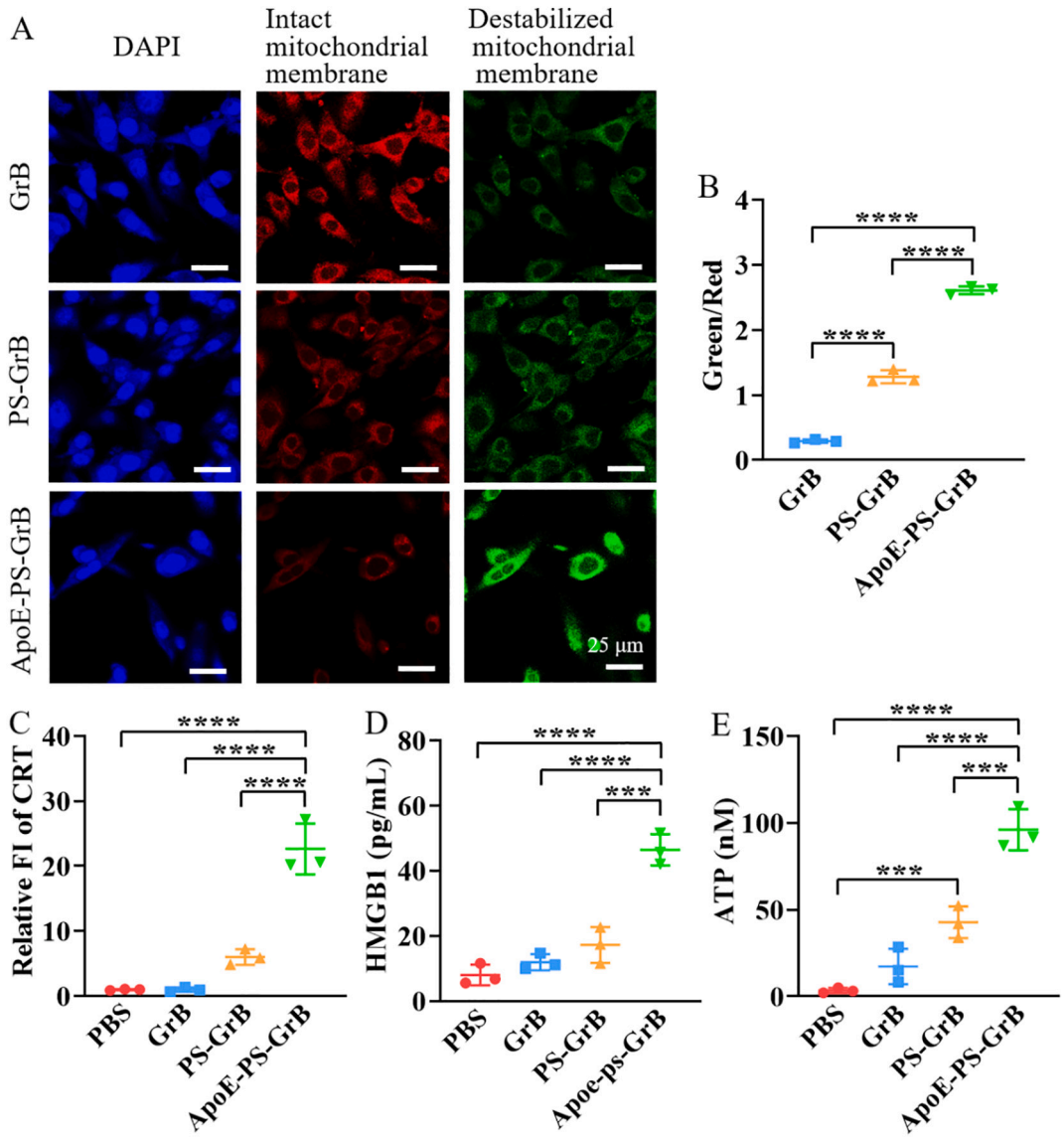

Fig. 3. The effect of ApoE-PS-GrB, PS-GrB and free GrB on mitochondria and release of damage-associated molecular patterns (DAMPs) in LCPN cells at 24 h incubation ([GrB] = 30 nM). (A) CLSM observation of MitoCapture stained LCPN cells (red and green represent intact and destabilized mitochondrial membrane, respectively). (B) The fluorescence intensity ratio of destabilized to intact mitochondrial membrane (Green/Red) semi-quantified by Image J ($n = 3$). (C) Quantitative analysis of CRT exposure on LCPN cells. Concentrations of secreted HMGB1 (D) and ATP (E) in culture media. ***$p < 0.001$; ****$p < 0.0001$. (For interpretation of the references to colour in this figure legend, the reader is referred to the web version of this article.)

trigger calreticulin (CRT) expression on the surface of tumor cells [42]. In fact, CRT, ATP, and high mobility group box 1 (HMGB1) are considered as major biomarkers of immunogenic cell death (ICD) which can serve as an "eat me" signal to induce phagocytosis by the APCs (especially DCs) in tumor microenvironment [43]. To investigate the ICD induction effect of ApoE-PS-GrB in LCPN cells following 24 h incubation (GrB: 30 nM), CRT on LCPN cells as well as HMGB1 and ATP in the culture media were analyzed. The flow cytometric histograms showed that ApoE-PS-GrB dramatically up-regulated the CRT expression compared with free GrB and PS-GrB (Fig. S2). The semi-quantitative analyses revealed that ApoE-PS-GrB had 23.7 and 3.7-fold higher CRT expression over GrB and PS-GrB, respectively (Fig. 3C). HMGB1 proteins normally distributed in the nuclei would migrate outside of the cell, acting as a Toll-like receptor agonist to stimulate DC maturation, when the tumor cells underwent ICD [43]. ELISA results showed that ApoE-PS-GrB group secreted 3.9 and 2.7-fold higher HMGB1 than GrB and PS-GrB groups, respectively (Fig. 3D). Furthermore, ApoE-PS-GrB group displayed also 5.5 and 2.2-fold higher ATP secretion than free GrB and PS-GrB groups, respectively (Fig. 3E). These results support that ApoE-PS-GrB induces immunogenic death of LCPN glioma cells.

3.4. Immunotherapy of orthotopic LCPN glioma-bearing mice

Encouraged by its good BBB penetration, glioma-targetability and strong ICD induction, we hereby evaluated the *in vivo* performance and immunotherapeutic effects of ApoE-PS-GrB toward orthotopic LCPN glioma-bearing mice. The *in vivo* pharmacokinetics using CC-Cy5 as model protein showed that both ApoE-PS-CC and PS-CC had a long elimination half-life ($t_{1/2,\beta}$) and high area under the curve of ca. 6.5 h and 200 μg·h/mL, respectively (Fig. 4A). The biodistribution studies in orthotopic LCPN-bearing mice revealed that ApoE-PS-CC achieved a notable CC accumulation of 3.4% ID/g in the brain tumor at 12 h post *i.v.* injection, which was significantly higher than non-targeted PS-CC (**p) (Fig. S3). In comparison, minimal amount of CC was delivered by ApoE-PS-CC to the normal brain tissues (***p). These results confirm that ApoE-PS mediates effective BBB penetration and selective delivery of

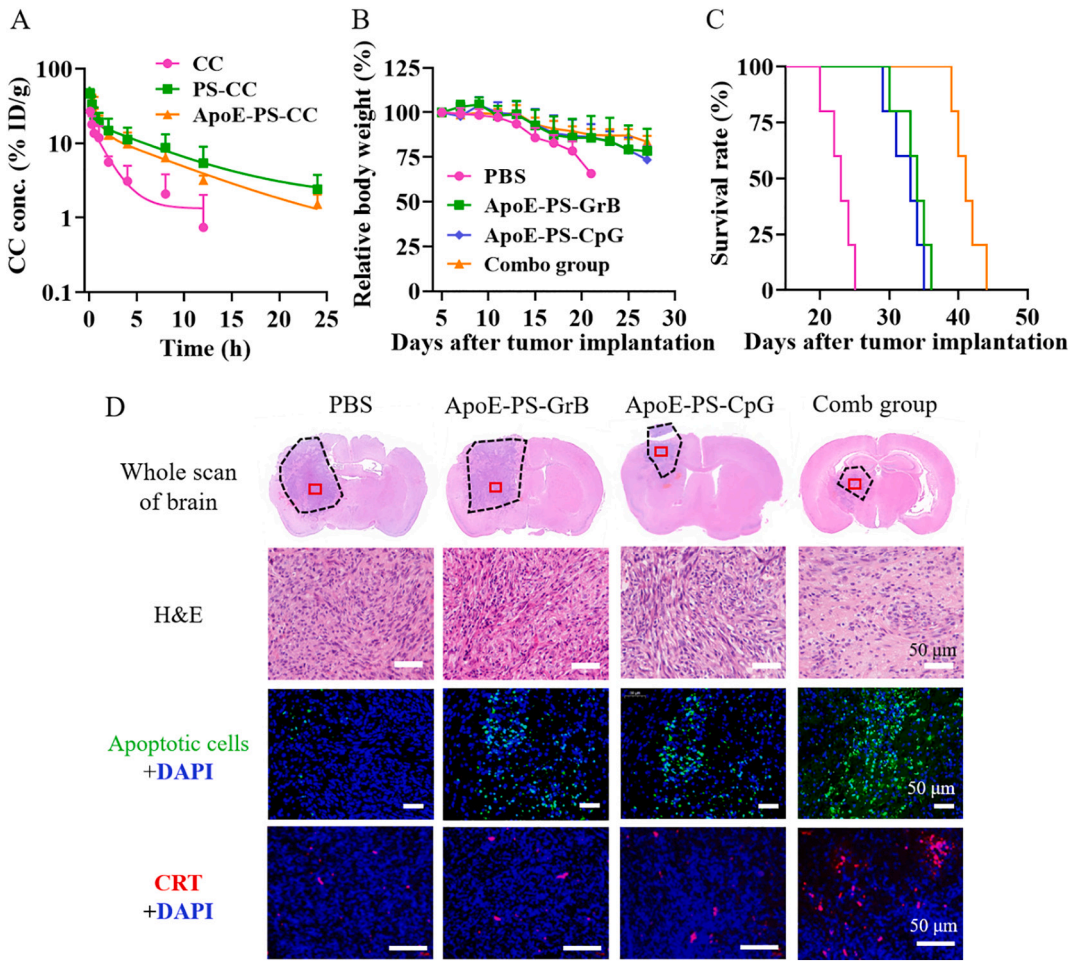

Fig. 4. *In vivo* pharmacokinetics and immunotherapy of protein loaded polymersomes. (A) *In vivo* pharmacokinetics of protein loaded polymersomes using CC-Cy5 as model protein. (B) Body weight change and (C) survival curves of orthotopic LCPN glioma-bearing mice ($n = 5$). The mice were *i.v.* injected with PBS, ApoE-PS-GrB (0.1 mg/kg), ApoE-PS-CpG (0.5 mg/kg), or combo group of ApoE-PS-GrB (0.1 mg/kg) + ApoE-PS-CpG (0.5 mg/kg) on day 5, 8, 11, and 14 after tumor implantation. Kaplan-Meier analysis: Combo group vs ApoE-PS-GrB or ApoE-PS-CpG: $^{**}p < 0.01$; ApoE-PS-GrB or ApoE-PS-CpG vs PBS: $^{**}p < 0.01$. (D) The tumor-containing brain tissue slices and tumor slices stained with H&E, TUNEL or anti-CRT antibody on day 20 post implantation.

proteins to glioblastoma. It should be noted that as for other nanosystems, both ApoE-PS-CC and PS-CC displayed a high accretion in the liver and spleen and there was no significant difference between ApoE-PS-CC and PS-CC in all major organs, indicating that ApoE on polymersomes does not increase its uptake in healthy tissues.

The immunotherapy of glioma might further be augmented by combining ApoE-PS-GrB with immunoadjuvants like CpG oligonucleotide (CpG) [25,26]. As an immune adjuvant, CpG can activate DCs and recruit CTLs, and has achieved exciting results in glioma treatment by i.c. injection or CED [44,45]. Of note, non-invasive administration of CpG, which is preferred, for boosting immune response in glioma therapy, has achieved little success. We have shown previously that CpG loaded in polymersomes exhibited improved dendritic cell maturation compared with free CpG [46]. Here, to enhance its BBB-permeability and bioavailability, we prepared ApoE-functionalized CpG nanoformulation, ApoE-PS-CpG, similar to previous report [46]. ApoE-PS-CpG had a high CpG loading efficiency of over 93% at theoretical loading contents of 10–20 wt%, decent sizes of ca. 45 nm (Fig. S4A) and weakly negative zeta potential of ca. −5 mV. It is shown that receptors like LDLR, LRP-1 and LRP-2 have elevated expression on DCs and macrophages [47]. *In vitro* BMDC stimulation results displayed that ApoE-PS-CpG induced ca. 60% BMDC maturation ($CD11c^{+}CD80^{+}CD86^{+}$) even at a low CpG concentration of 0.4 μg/mL, which was significantly higher than all other groups including empty ApoE-PS, free CpG, and PS-CpG (Fig. S4B). Moreover, treatment of BMDMs with ApoE-PS-CpG significantly decreased the suppressive M2 phenotype (M2M, $F4/80^{+}CD206^{+}$) from 56% (PBS group) to 36% (Fig. S4C).

The orthotopic murine LCPN glioma mouse model was established by intracranial (i.c.) injection of LCPN cells into C57BL/6 mice. On day 5 post tumor implantation, the mice were randomly assigned into four groups ($n = 9$) and *i.v.* injected with PBS, ApoE-PS-GrB (0.1 mg/kg), ApoE-PS-CpG (0.5 mg/kg), or combo group of ApoE-PS-GrB (0.1 mg/kg) + ApoE-PS-CpG (0.5 mg/kg). LCPN glioma was highly malignant. The mice receiving only PBS exhibited rapid loss in body weight (Fig. 4B), owing to violent proliferation and invasion of LCPN cells into brain tissue. Previously, we have shown that progression of LCPN tumor positively correlated with loss of body weight. The body weight loss was retarded by all three treatments (Fig. 4B), indicating effective suppression of glioma invasion. Kaplan-Meier survival curves unveiled that both ApoE-PS-GrB and ApoE-PS-CpG substantially extended the survival time of LCPN glioma-bearing mice ($^{**}p$) (Fig. 4C). More interestingly, the combo group of ApoE-PS-GrB + ApoE-PS-CpG induced further significant improvement of the survival rate compared with ApoE-PS-GrB or ApoE-PS-CpG monotherapy ($^{**}p$). The antitumor effect of ApoE-PS-CpG arises from its strong stimulation of anticancer immune responses in the glioma [48]. The above results point out that ApoE-PS-GrB is able to permeate BBB via LDLRs-mediated transcytosis, selectively accumulate in the LCPN tumor and be endocytosed by LCPN cells via binding to LDLRs, and promote release of GrB in the cytosol as a result of reduction-

triggered cleavage of disulfide crosslinks, specifically inducing immunogenic cell death of LCPN tumor cells.

Hematoxylin-eosin (H&E) staining of the tumor-containing brain slices illustrated that among all groups, the combo group had the smallest tumor in the brain and the least dense tumor texture (Fig. 4D). Terminal deoxynucleotidyl transferase-mediated nick end labeling (TUNEL) staining also showed much more extensive cell apoptosis for the combo group than both ApoE-PS-GrB and ApoE-PS-CpG groups. The anti-CRT antibody staining displayed that the combo group was the most capable in releasing tumor associated antigens *in vivo* (Fig. 4D). Of note, the tumor slice of PBS group showed a small amount of cell death and these dead tumor cells were immunogenic, as shown by the CRT expression. The delivery of ApoE-PS-CpG to orthotopic LCPN tumor would activate DCs and present antigens to $CD8^+$ T cells, leading to anti-tumor immune response. It is important to note that all treatments did not cause damage to the major organs such as heart, liver, spleen, lung and kidney (Fig. S5), despite the fact that polymersomal formulations with or without ApoE had a high accumulation in the liver and spleen (Fig. S3). The reason for this observed low off-target toxicity for ApoE-PS-GrB is likely because of its inferior cell uptake in the healthy tissues. ApoE-PS-GrB induces cytotoxic effects only when taking up by cells and releasing GrB to the cytosols. Hence, the *i.v.* administration of ApoE-

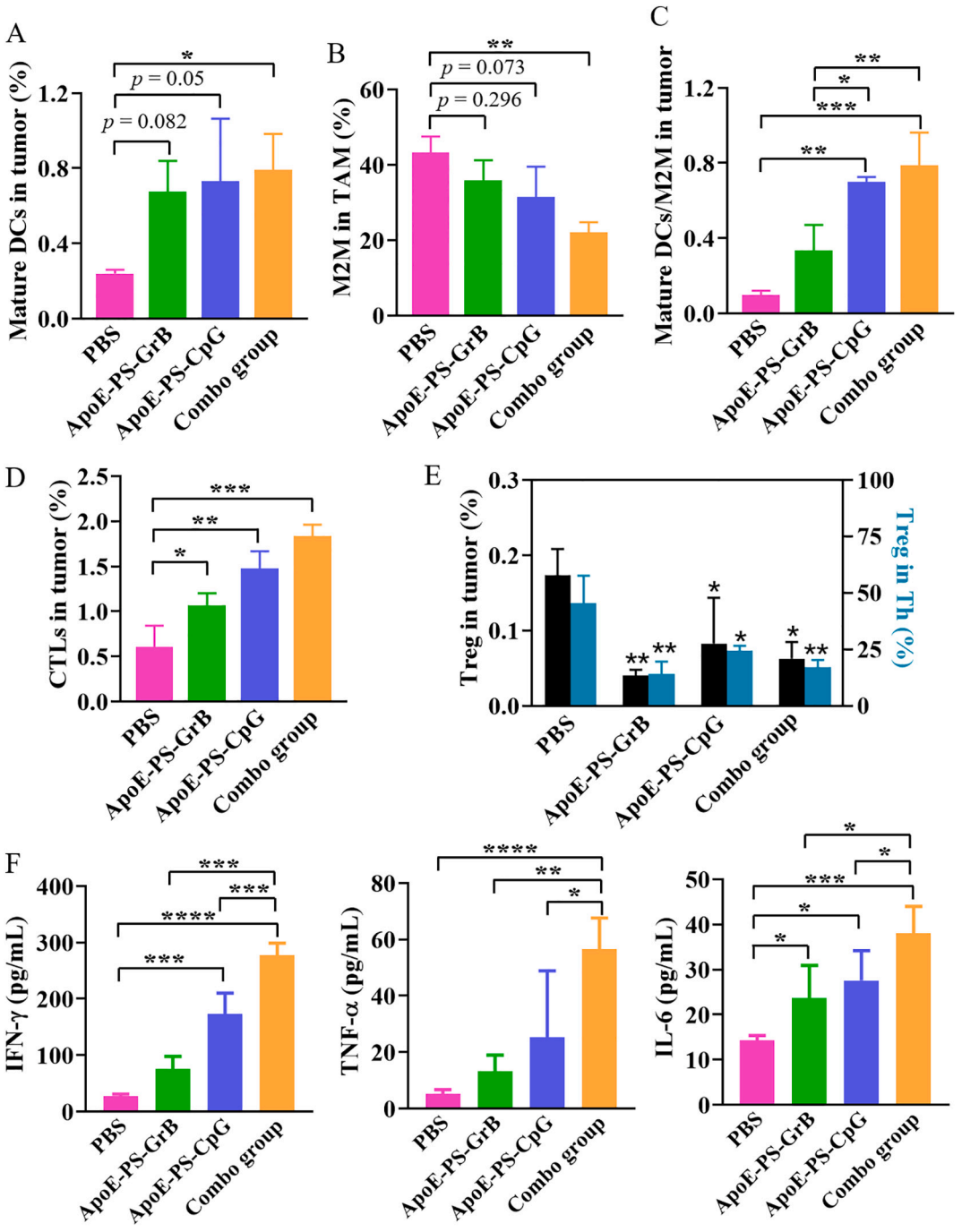

Fig. 5. Immunological analyses of orthotopic LCPN-bearing mice after immunotherapy with ApoE-PS-GrB and ApoE-PS-CpG. Flow cytometry quantification of mature DCs ($CD11c^+CD80^+CD86^+$) (A), M2 phenotype ($CD11b^+F4/80^+CD206^+$) of total TAM (B), mature DCs/M2M (C), CTLs ($CD3^+CD8^+$ T cells) (D), and T_{reg} ($CD3^+CD4^+CD25^+$ T cells) (E) in the tumors ($n = 3$). (F) The plasma concentrations of TNF-α, IFN-γ and IL-6 ($n = 4$). *$p < 0.05$; **$p < 0.01$; ***$p < 0.001$, ****$p < 0.0001$.

PS-GrB and ApoE-PS-CpG provides a safe and efficient immunotherapeutic treatment for murine orthotopic glioma.

3.5. Immunological analyses

To unveil the role of activated immune cells for boosting immune response in anti-glioma therapy, the tumor infiltrating immune cells from different treatment groups on day 20 were quantified using flow cytometric analysis. Fig. 5A shows that ApoE-PS-GrB, ApoE-PS-CpG and the combo group all led to considerable increase of mature DCs. DCs can recognize danger signals (e.g. CRT and HMGB1 released by the dying tumor cells) or exogenous CpG [49], and are stimulated into maturation showing elevated expression of molecules involved in antigen presentation such as MHC II and co-stimulatory CD80 and CD86, which play a crucial role in activating T cells [50]. Interestingly, though three treatment groups had similar total tumor-associated macrophages (TAM) (Fig. S6A), the proportion of the immune suppressive M2M in TAM decreased from PBS, ApoE-PS-GrB, ApoE-PS-CpG, to the combo group (from 43%, 35%, 31%, to 21%, respectively) (Fig. 5B). Notably, the ratio of mature DC to M2M for PBS, ApoE-PS-GrB, ApoE-PS-CpG, and combo groups increased from 0.10 to 0.33, 0.70 and 0.79, respectively (Fig. 5C). Furthermore, ApoE-PS-GrB, ApoE-PS-CpG, or combo group significantly elevated $CD3^+CD8^+$ T cells (CTLs) contents in tumor compared with PBS (1.8, 2.5 and 3.1-fold) (Fig. 5D). Encouragingly, CTLs in ApoE-PS-CpG group were in similar level as reported for GL261 mouse model i.c. injected with CpG [51]. The intratumor injection of CpG to 4 T1 breast tumor and B16 melanoma could also generate abundant tumor infiltrating CTLs [52–54], though systemic injection had no therapeutic effect in B16 melanoma model [53]. Even though $CD3^+CD4^+$ T cells (T_h) had no difference among groups (Fig. S6B), the percentages of immunosuppressive T_{reg} in tumor and T_{reg} in T_h noticeably reduced in all treatment groups (Fig. 5E). Hence, the combo group treatment significantly elevated mature DCs and CTLs in tumors that are in a serious exhaustion state in glioma, and reduced the immunosuppressive T_{reg} and M2M, thus remodeling the tumor microenvironment to a favorable immune condition.

The plasma cytokines of the mice such as interferon gamma (IFN-γ), tumor necrosis factor alpha (TNF-α) and interleukin-6 (IL-6), which play crucial roles in the cytotoxic functions of CTLs, were quantified using ELISA kits (Fig. 5F). Compared to PBS group, ApoE-PS-GrB induced while significant increase of IL-6 (*p), only moderate increase in both IFN-γ and TNF-α. ApoE-PS-CpG could stimulate significantly higher production of IFN-γ (***p) and IL-6 (*p) but not TNF-α. In comparison, the combo group induced highly significant stimulation of all three cytokines, IFN-γ (****p), TNF-α (****p), and IL-6 (***p), which were 10.2, 13.1, and 2.7-fold that of PBS group, respectively. These cytokines can recruit and activate DCs and T cells to glioma. These results highlight that *i.v.* injection of ApoE-PS-GrB and ApoE-PS-CpG is able to trigger both innate and adaptive immune responses in the TME by recruiting and activating DCs and cytotoxic T cells, and by decreasing immunosuppressive M2M and T_{reg} as well as secreting TNF-α, IFN-γ and IL-6, inducing enhanced immunotherapy of murine orthotopic glioma. This study proves that ApoE-PS-GrB can induce ICD of glioma, which combining with ApoE-PS-CpG stimulates strong anti-tumor immune responses. It is most likely that by optimizing their dose, dosing scheme and administration method (e.g. intranasal administration), we may achieve further enhanced anti-glioma therapy.

4. Conclusion

We have demonstrated that ApoE-mediated systemic nanodelivery of granzyme B and CpG induces a safe and enhanced immunotherapy of malignant murine LCPN glioma. LDLRs-targeting ApoE-PS-GrB not only exhibits enhanced BBB permeability and uptake by LDLRs-overexpressing LCPN cancer cells but also induces significantly more extensive immunogenic cell death compared with free GrB and non-targeting PS-GrB. ApoE-PS-CpG, on the other hand, enhances uptake by DCs and more efficiently triggers DC maturation ($CD80^+CD86^+$) than free CpG and PS-CpG. Of note, combination of ApoE-PS-GrB and ApoE-PS-CpG promotes effective remodeling of suppressive immune microenvironment in LCPN glioma by (i) generating tumor antigens, (ii) increasing mature DCs and CTLs while decreasing Treg and M2M in the tumor, and (iii) increasing secretion of TNF-α, IFN-γ and IL-6 cytokines, leading to enhanced glioma inhibition and significant survival benefits over monotherapy. This ApoE-mediated systemic nanodelivery of granzyme B and CpG provides a novel and non-invasive immunotherapeutic strategy for malignant glioma, which combining with immune checkpoint inhibitors such as anti-PD-1 and anti-PD-L1 may further boost glioma therapy.

Credit author statement

J.J. Wei designed and carried out the experiments and drafted the paper; D. Wu and J. Chen established the LCPN mouse model; B·B Guo and J.J. Jiang carried out the biodistribution experiment and analysis; Y. Shao and J. P. Zhang conducted immunological measurements and analyses; F. H. Meng and Z. Y. Zhong co-supervised the work and revised the paper.

Acknowledgements

This work is supported by research grants from the National Natural Science Foundation of China (NSFC 52033006, 51861145310, 51633005) and the National Key R&D Program of China (2016YFA0503100).

Appendix A. Supplementary data

Supplementary data to this article can be found online at https://doi.org/10.1016/j.jconrel.2022.04.048.

References

[1] C. Neftel, J. Laffy, M.G. Filbin, T. Hara, M.E. Shore, G.J. Rahme, A.R. Richman, D. Silverbush, M.L. Shaw, C.M. Hebert, J. Dewitt, S. Gritsch, E.M. Perez, L.N. G. Castro, X.Y. Lan, N. Druck, C. Rodman, D. Dionne, A. Kaplan, M.S. Bertalan, J. Small, K. Pelton, S. Becker, D. Bonal, Q.D. Nguyen, R.L. Servis, J.M. Fung, R. Mylvaganam, L. Mayr, J. Gojo, C. Haberler, R. Geyeregger, T. Czech, I. Slavc, B. V. Nahed, W.T. Curry, B.S. Carter, H. Wakimoto, P.K. Brastianos, T.T. Batchelor, A. Stemmer-Rachamimov, M. Martinez-Lage, M.P. Frosch, I. Stamenkovic, N. Riggi, E. Rheinbay, M. Monje, O. Rozenblatt-Rosen, D.P. Cahill, A.P. Patel, T. Hunter, I. M. Verma, K.L. Ligon, D.N. Louis, A. Regev, B.E. Bernstein, I. Tirosh, M.L. Suva, An integrative model of cellular states, plasticity, and genetics for glioblastoma, Cell 178 (2019) 835–849.

[2] P.Y. Wen, M. Weller, E.Q. Lee, B.M. Alexander, J.S. Barnholtz-Sloan, F.P. Barthel, T.T. Batchelor, R.S. Bindra, S.M. Chang, E.A. Chiocca, T.F. Cloughesy, J.F. DeGroot, E. Galanis, M.R. Gilbert, M.E. Hegi, C. Horbinski, R.Y. Huang, A.B. Lassman, E. Le Rhun, M. Lim, M.P. Mehta, I.K. Mellinghoff, G. Minniti, D. Nathanson, M. Platten, M. Preusser, P. Roth, M. Sanson, D. Schiff, S.C. Short, M.J.B. Taphoorn, J.C. Tonn, J. Tsang, R.G.W. Verhaak, A. von Deimling, W. Wick, G. Zadeh, D.A. Reardon, K. D. Aldape, M.J. van den Bent, Glioblastoma in adults: a Society for Neuro-Oncology (SNO) and European Society of Neuro-Oncology (EANO) consensus review on current management and future directions, Neuro-Oncology 22 (2020) 1073–1113.

[3] D. Furtado, M. Bjornmalm, S. Ayton, A.I. Bush, K. Kempe, F. Caruso, Overcoming the blood-brain barrier: the role of nanomaterials in treating neurological diseases, Adv. Mater. 30 (2018) 1801362.

[4] L. Hua, Z. Wang, L. Zhao, H.L. Mao, G.H. Wang, K.R. Zhang, X.J. Liu, D.M. Wu, Y. L. Zheng, J. Lu, R.T. Yu, H.M. Liu, Hypoxia-responsive lipid-poly-(hypoxic radiosensitized polyprodrug) nanoparticles for glioma chemo- and radiotherapy, Theranostics 8 (2018) 5088–5105.

[5] S. Ruan, Y. Zhou, X. Jiang, H. Gao, Rethinking CRITID procedure of brain targeting drug delivery: circulation, blood brain barrier recognition, intracellular transport, diseased cell targeting, internalization, and drug release, Adv. Sci. 8 (2021) 2004025.

[6] J.H. Sampson, M.D. Gunn, P.E. Fecci, D.M. Ashley, Brain immunology and immunotherapy in brain tumours, Nat. Rev. Cancer 20 (2020) 12–25.

[7] H.X. Wang, T. Xu, Q.L. Huang, W.L. Jin, J.X. Chen, Immunotherapy for malignant glioma: current status and future directions, Trends Pharmacol. Sci. 41 (2020) 123–138.

[8] S.J. Peng, F.F. Xiao, M.W. Chen, H.L. Gao, Tumor-microenvironment-responsive nanomedicine for enhanced cancer immunotherapy, Adv. Sci. 9 (2022) 2103836.

[9] A. Kerstetter-Fogle, S. Shukla, C. Wang, V. Beiss, P.L.R. Harris, A.E. Sloan, N. F. Steinmetz, Plant virus-like particle in situ vaccine for intracranial glioma immunotherapy, Cancers 11 (2019) 515.
[10] M. Lim, Y.X. Xia, C. Bettegowda, M. Weller, Current state of immunotherapy for glioblastoma, Nat. Rev. Clin. Oncol. 15 (2018) 422–442.
[11] J. Zhang, C. Chen, A. Li, W. Jing, P. Sun, X. Huang, Y. Liu, S. Zhang, W. Du, R. Zhang, Y. Liu, A. Gong, J. Wu, X. Jiang, Immunostimulant hydrogel for the inhibition of malignant glioma relapse post-resection, Nat. Nanotechnol. 16 (2021) 538–548.
[12] C.M. Jackson, J. Choi, M. Lim, Mechanisms of immunotherapy resistance: lessons from glioblastoma, Nat. Immunol. 20 (2019) 1100–1109.
[13] B. Weenink, P.J. French, P.A.E.S. Smitt, R. Debets, M. Geurts, Immunotherapy in glioblastoma: current shortcomings and future perspectives, Cancers 12 (2020) 751.
[14] D.F. Quail, J.A. Joyce, The microenvironmental landscape of brain tumors, Cancer Cell 31 (2017) 326–341.
[15] W. Niu, Q. Xiao, X. Wang, J. Zhu, J. Li, X. Liang, Y. Peng, C. Wu, R. Lu, Y. Pan, J. Luo, X. Zhong, H. He, Z. Rong, J. Fan, Y. Wang, Abiomimetic drug delivery system by integrating grapefruit extracellular vesicles and doxorubicin-loaded heparin-based nanoparticles for glioma therapy, Nano Lett. 21 (2021) 1484–1492.
[16] N.B. Roberts, A. Alqazzaz, J.R. Hwang, X.L. Qi, A.D. Keegan, A.J. Kim, J. A. Winkles, G.F. Woodworth, Oxaliplatin disrupts pathological features of glioma cells and associated macrophages independent of apoptosis induction, J. Neuro-Oncol. 140 (2018) 497–507.
[17] B. Du, D.J. Waxman, Medium dose intermittent cyclophosphamide induces immunogenic cell death and cancer cell autonomous type I interferon production in glioma models, Cancer Lett. 470 (2020) 170–180.
[18] J. Kuang, W. Song, J. Yin, X. Zeng, S. Han, Y.P. Zhao, J. Tao, C.J. Liu, X.H. He, X. Z. Zhang, iRGD modified chemo-immunotherapeutic nanoparticles for enhanced immunotherapy against glioblastoma, Adv. Funct. Mater. 28 (2018) 1800025.
[19] H. Xiao, R. Qi, T. Li, S.G. Awuah, Y. Zheng, W. Wei, X. Kang, H. Song, Y. Wang, Y. Yu, M.A. Bird, X. Jing, M.B. Yaffe, M.J. Birrer, P.P. Ghoroghchian, Maximizing synergistic activity when combining RNAi and platinum-based anticancer agents, J. Am. Chem. Soc. 139 (2017) 3033–3044.
[20] C. Zhou, Y.F. Xia, Y.H. Wei, L. Cheng, J.J. Wei, B.B. Guo, F.H. Meng, S.P. Cao, J.C. M. van Hest, Z.Y. Zhong, GE11 peptide-installed chimaeric polymersomes tailor-made for high-efficiency EGFR-targeted protein therapy of orthotopic hepatocellular carcinoma, Acta Biomater. 113 (2020) 512–521.
[21] X.H. Si, S. Ma, Y. Xu, D. Zhang, N. Shen, H.Y. Yu, Y. Zhang, W.T. Song, Z.H. Tang, X. Chen, Hypoxia-sensitive supramolecular nanogels for the cytosolic delivery of ribonuclease A as a breast cancer therapeutic, J. Control. Release 320 (2020) 83–95.
[22] A.Y. Tsidulko, C. Bezier, G. de la Bourdonnaye, A.V. Suhovskih, T.M. Pankova, G. M. Kazanskaya, S.V. Aidagulova, E.V. Grigorieva, Conventional anti-glioblastoma chemotherapy affects proteoglycan composition of brain extracellular matrix in rat experimental model in vivo, Front. Pharmacol. 9 (2018) 13.
[23] C.W. Lu, J.D. Klement, M.L. Ibrahim, W. Xiao, P.S. Redd, A. Nayak-Kapoor, G. Zhou, K.B. Liu, Type I interferon suppresses tumor growth through activating the STAT3-granzyme B pathway in tumor-infiltrating cytotoxic T lymphocytes, J. Immunother. Cancer 7 (2019) 157.
[24] Y.L.P. Ow, D.R. Green, Z. Hao, T.W. Mak, Cytochrome C: functions beyond respiration, Nat. Rev. Mol. Cell Biol. 9 (2008) 532–542.
[25] P. Kadiyala, D. Li, F.M. Nunez, D. Altshuler, R. Doherty, R. Kuai, M.Z. Yu, N. Kamran, M. Edwards, J.J. Moon, P.R. Lowenstein, M.G. Castro, A. Schwendeman, High-density lipoprotein-mimicking nanodiscs for chemo-immunotherapy against glioblastoma multiforme, ACS Nano 13 (2019) 1365–1384.
[26] Y. Chao, C. Liang, H.Q. Tao, Y.R. Du, D. Wu, Z.L. Dong, Q.T. Jin, G.B. Chen, J. Xu, Z.S. Xiao, Q. Chen, C. Wang, J. Chen, Z. Liu, Localized cocktail chemoimmunotherapy after in situ gelation to trigger robust systemic antitumor immune responses, Sci. Adv. 6 (2020) eaaz4204.
[27] G. Lollo, M. Vincent, G. Ullio-Gamboa, L. Lemaire, F. Franconi, D. Couez, J.-P. Benoit, Development of multifunctional lipid nanocapsules for the co-delivery of paclitaxel and CpG-ODN in the treatment of glioblastoma, Int. J. Pharm. 495 (2015) 972–980.
[28] A. Carpentier, P. Metellus, R. Ursu, S. Zohar, F. Lafitte, M. Barrié, Y. Meng, M. Richard, C. Parizot, F. Laigle-Donadey, G. Gorochov, D. Psimaras, M. Sanson, A. Tibi, O. Chinot, A. Carpentier, Intracerebral administration of CpG oligonucleotide for patients with recurrent glioblastoma: a phase II study, Neuro-oncology 12 (2010) 401–408.
[29] N. Hartl, F. Adams, O.M. Merkel, From adsorption to covalent bonding: Apolipoprotein E functionalization of polymeric nanoparticles for drug delivery across the blood-brain barrier, Adv. Ther. 4 (2021) 2000092.
[30] Y.N. Shi, Y. Jiang, J.S. Cao, W.J. Yang, J. Zhang, F.H. Meng, Z.Y. Zhong, Boosting RNAi therapy for orthotopic glioblastoma with nontoxic brain-targeting chimaeric polymersomes, J. Control. Release 292 (2018) 163–171.
[31] Y. Jiang, J. Zhang, F.H. Meng, Z.Y. Zhong, Apolipoprotein E peptide-directed chimeric polymersomes mediate an ultrahigh-efficiency targeted protein therapy for glioblastoma, ACS Nano 12 (2018) 11070–11079.
[32] Y. Jiang, W.J. Yang, J. Zhang, F.H. Meng, Z.Y. Zhong, Protein toxin chaperoned by LRP-1-targeted virus-mimicking vesicles induces high-efficiency glioblastoma therapy in vivo, Adv. Mater. 30 (2018) 1800316.
[33] S. Elmore, Apoptosis: a review of programmed cell death, Toxicol. Pathol. 35 (2007) 495–516.
[34] Y.N. Zhong, F.H. Meng, W. Zhang, B. Li, J.C.M. van Hest, Z.Y. Zhong, CD44-targeted vesicles encapsulating granzyme B as artificial killer cells for potent inhibition of human multiple myeloma in mice, J. Control. Release 320 (2020) 421–430.
[35] W.J. Yang, Y.H. Wei, L. Yang, J. Zhang, Z.Y. Zhong, G. Storm, F.H. Meng, Granzyme B-loaded, cell-selective penetrating and reduction-responsive polymersomes effectively inhibit progression of orthotopic human lung tumor in vivo, J. Control. Release 290 (2018) 141–149.
[36] Y.H. Wei, X.L. Gu, Y.P. Sun, F.H. Meng, G. Storm, Z.Y. Zhong, Transferrin-binding peptide functionalized polymersomes mediate targeted doxorubicin delivery to colorectal cancer in vivo, J. Control. Release 319 (2020) 407–415.
[37] W. Gu, J. An, H. Meng, N. Yu, Y. Zhong, F. Meng, Y. Xu, J.J.L.M. Cornelissen, Z. Zhong, CD44-specific A6 short peptide boosts targetability and anticancer efficacy of polymersomal epirubicin to orthotopic human multiple myeloma, Adv. Mater. 31 (2019) 1904742.
[38] W. Yang, Y. Xia, Y. Zou, F. Meng, J. Zhang, Z. Zhong, Bioresponsive chimaeric nano-polymersomes enable targeted and efficacious protein therapy for human lung cancers in vivo, Chem. Mater. 29 (2017) 8757–8765.
[39] A. Böckenhoff, S. Cramer, P. Wölte, S. Knieling, C. Wohlenberg, V. Gieselmann, H.-J. Galla, U. Matzner, Comparison of five peptide vectors for improved brain delivery of the lysosomal enzyme arylsulfatase A, J. Neurosci. 34 (2014) 3122–3129.
[40] W. He, X. Li, M. Morsch, M. Ismail, Y. Liu, F.U. Rehman, D. Zhang, Y. Wang, M. Zheng, R. Chung, Y. Zou, B. Shi, Brain-targeted codelivery of Bcl-2/Bcl-xl and Mcl-1 inhibitors by biomimetic nanoparticles for orthotopic glioblastoma therapy, ACS Nano 16 (2022) 6293–6308.
[41] W. Gu, F. Meng, R. Haag, Z. Zhong, Actively targeted nanomedicines for precision cancer therapy: concept, construction, challenges and clinical translation, J. Control. Release 329 (2021) 676–695.
[42] Q.Z. Jiang, C. Zhang, H.L. Wang, T. Peng, L. Zhang, Y. Wang, W.D. Han, C.M. Shi, Mitochondria-targeting immunogenic cell death inducer improves the adoptive T-cell therapy against solid tumor, Front. Oncol. 9 (2019) 1196.
[43] B. Feng, Z.F. Niu, B. Hou, L. Zhou, Y.P. Li, H.J. Yu, Enhancing triple negative breast cancer immunotherapy by ICG-templated self-assembly of paclitaxel nanoparticles, Adv. Funct. Mater. 30 (2020) 1906605.
[44] G. Lollo, M. Vincent, G. Ullio-Gamboa, L. Lemaire, F. Franconi, D. Couez, J. P. Benoit, Development of multifunctional lipid nanocapsules for the co-delivery of paclitaxel and CpG-ODN in the treatment of glioblastoma, Int. J. Pharm. 495 (2015) 972–980.
[45] M. Ouyang, E. White, H. Ren, Q. Guo, I. Zhang, H. Gao, S. Yanyan, X. Chen, Y. Weng, A.C. Carvalho da Fonseca, S. Shah, E. Manuel, L. Zhang, S. Vonderfecht, D. Alizadeh, J. Berlin, B. Badie, Metronomic doses of temozolomide enhance the efficacy of carbon nanotube CpG immunotherapy in an invasive glioma model, PLoS One 11 (2016) e0148139.
[46] Y. Xia, J. Wei, S. Zhao, B. Guo, F. Meng, B. Klumperman, Z. Zhong, Systemic administration of polymersomal oncolytic peptide LTX-315 combining with CpG adjuvant and anti-PD-1 antibody boosts immunotherapy of melanoma, J. Control. Release 336 (2021) 262–273.
[47] L. Galluzzi, A. Buque, O. Kepp, L. Zitvogel, G. Kroemer, Immunogenic cell death in cancer and infectious disease, Nat. Rev. Immunol. 17 (2017) 97–111.
[48] J. Wei, D. Wu, S. Zhao, Y. Shao, Y. Xia, D. Ni, X. Qiu, J. Zhang, J. Chen, F. Meng, Z. Zhong, Immunotherapy of malignant glioma by noninvasive administration of TLR9 agonist CpG nano-immunoadjuvant, Adv. Sci. (2022) 2103689.
[49] J. Ming, J.J. Zhang, Y.R. Shi, W.H. Yang, J.C. Li, D. Sun, S.J. Xiang, X.L. Chen, L. F. Chen, N.F. Zheng, A trustworthy CpG nanoplatform for highly safe and efficient cancer photothermal combined immunotherapy, Nanoscale 12 (2020) 3916–3930.
[50] S. Yüksel, M. Pekcan, N. Puralı, G. Esendağlı, E. Tavukçuoğlu, V. Rivero-Arredondo, L. Ontiveros-Padilla, C. López-Macías, S. Şenel, Development and in vitro evaluation of a new adjuvant system containing Salmonella Typhi porins and chitosan, Int. J. Pharm. 578 (2020) 119129.
[51] D. Alizadeh, L.Y. Zhang, C.E. Brown, O. Farrukh, M.C. Jensen, B. Badie, Induction of anti-glioma natural killer cell response following multiple low-dose intracerebral CpG therapy, Clin. Cancer Res. 16 (2010) 3399–3408.
[52] Z. Wang, Y. Zhang, Z. Liu, K. Dong, C. Liu, X. Ran, F. Pu, E. Ju, J. Ren, X. Qu, A bifunctional nanomodulator for boosting CpG-mediated cancer immunotherapy, Nanoscale 9 (2017) 14236–14247.
[53] M.J. Reilley, B. Morrow, C.R. Ager, A. Liu, D.S. Hong, M.A. Curran, TLR9 activation cooperates with T cell checkpoint blockade to regress poorly immunogenic melanoma, J. Immunother. Cancer 7 (2019) 323.
[54] Y. Chao, L.G. Xu, C. Liang, L.Z. Feng, J. Xu, Z.L. Dong, L.L. Tian, X. Yi, K. Yang, Z. Liu, Combined local immunostimulatory radioisotope therapy and systemic immune checkpoint blockade imparts potent antitumour responses, Nat. Biomed. Eng. 2 (2018) 611–621.